Journal of Physics: Conference Series

PAPER • OPEN ACCESS

Numerical Simulation of rivulet build up via lubrication equations

To cite this article: N Suzzi and G Croce 2017 *J. Phys.: Conf. Ser.* **923** 012020

IOP Conf. Series: Journal of Physics: Conf. Series **923** (2017) 012020 doi:10.1088/1742-6596/923/1/012020

Numerical simulation of rivulet build up via lubrication equations

N Suzzi[1] **and G Croce**[1]

[1]DPIA - Dipartimento Politecnico di Ingegneria e Architettura - Universitá di Udine - Via delle Scienze - 33100 - Udine (UD) - Italy

E-mail: giulio.croce@uniud.it

Abstract. A number of engineering problems involve the evolution of a thin layer of liquid over a non-wettable substrate. For example, CO2 chemical absorption is carried out in packed columns, where post-combustion CO2 flows up while liquid solvent falls down through a collection of corrugated sheets. Further application include, among others, in-flight icing simulations, moisture condensation on de-humidifier fins, fogging build up and removal. Here, we present a development of an in-house code solving numerically the 2D lubrication equation for a film flowing down an inclined plate. The disjoining pressure approach is followed, in order to model both the contact line discontinuity and the surface wettability. With respect to the original implementation, the full modeling of capillary pressure terms according to Young-Laplace relation allows to investigate contact angles close to $\pi/2$. The code is thus validated with literature numerical results, obtained by a fully 3D approach (VOF), showing satisfying agreement despite a strong reduction in terms of computational cost. Steady and unsteady wetting dynamics of a developing rivulet are investigated (and validated) under different load conditions and for different values of the contact angles.

1. Introduction

The evolution of a thin layer of liquid over a non-wettable surface is a complex phenomenon, involving transition between still/moving droplet, rivulet and continuous film patterns, with physical discontinuities induced by moving contact lines. On the other side, a number of engineering problems requires the knowledge of the liquid distribution over a solid substrate. For example, in-flight icing on aircraft surface is driven by the evolution of a water layer fed by super-cooled drops from the cloud. The liquid distribution, which depends on the cloud water content and the fluid flow field and temperature, influences the location and shape of ice accretion areas, which in turn greatly affect the aircraft aerodynamics. Fogging and defogging of a car windshield or heat transfer on dehumidifier fin surfaces are also affected by condensation and evaporation phenomena with droplets growth, coalescence and motion over solid substrates. Several works concerning these topics are available in literature [1–3].

Even chemical absorption of post-combustion carbon dioxide involves the evolution of a thin layer of liquid. In fact, gas CO_2 flows up while a liquid solvent, which has to capture carbon, flows down through a packed column, composed by a collection of structured corrugated sheets. The absorption process is more efficient when the packed layers are covered by a continuous film, rather than drops or rivulets. Both numerical and experimental literature are available, but it is clearly difficult to look inside the packed columns, making the numerical approach much more

suitable. Moreover, most of the above mentioned problems are inherently multiscale: a packed column may have a diameter of 10 m, while the characteristic dimension of structured packing is of the order of 20 cm and the film height may be less than a millimeter [4]; thus, a full CFD approach is typically limited to the investigation of a single facet of the problem: most analysis, in fact, are focused on the hydrodynamic behavior of a liquid along plane surfaces. In particular, Hoffmann et al. [5] validated the Volume Of Fluid (VOF) method for a film flowing down an inclined plate with walls at the lateral boundaries, constructing a two fluid model (gas-liquid) and comparing numerical results with experimental evidences. Singh et al. presented a number of numerical results in [4], where the authors considered the same test case of [5] and adopted a fully 3D approach (VOF) as well, looking for the influence of solvent properties and flow rate. There are other literature works involving absorption and distillation through structured packing [6–8], which focus on numerical simulation of a falling film driven by gravity and shear using VOF method.

Here, we are following a different approach. In order to reduce the computational effort for the simulation of the film dynamics, we consider the 2D lubrication equation, solved numerically by means of Finite Volume Method (FVM). The idea is to look for an efficient, yet accurate model that could be coupled with a full CFD of the core flow, in order to investigate simultaneously both the large scales of the device (the full packed column, or the full wing or nacelle for a in-flight icing problem) and the smaller scale of the film.

Lubrication theory has been widely used in open literature for describing droplet spreading on non-wettable surfaces or flowing film dynamics [9–16], but the small-slope approximation when calculating free surface curvature does not allow to investigate contact angle higher than 20°.

In the present work, the implementation of the capillary pressure according to the membranal theory allows to investigate equilibrium contact angle up to 60°, thus making it suitable for a larger number of practical applications.

An in-house, fully implicit code was built and used for the current simulations. Precursor film together with disjoining pressure model allow for the modeling of the surface wettability (i.e. equilibrium contact angle), as also made in [9, 10, 12, 16]. The FVM solver code is first validated with literature numerical results involving rivulet build up and then applied to the case of a gravity driven film down an inclined plate, looking for useful information about wetting dynamics inside packed columns for CO_2 absorption applications.

2. Mathematical model

Consider a thin film of height h flowing along an inclined plate under the action of both gravity and shear, α being the plate inclination with respect to the horizontal and $\boldsymbol{\tau}$ the shear applied by an external gas flow. Let h_∞ and u_∞ be the undisturbed film height and velocity.

The lubrication theory describing the evolution of a thin layer of liquid over a solid substrate offers:

$$\frac{\partial h}{\partial t} = -\nabla \cdot \boldsymbol{Q} = -\nabla \cdot \left(-\frac{\nabla p}{3\,\mu}\, h^3 + \frac{\boldsymbol{\tau}}{2\,\mu}\, h^2 \right) \tag{1}$$

which is valid for low values of Reynolds number, $\mathrm{Re} = \rho\, u_\infty\, h_\infty / \mu \leq 1$.

The pressure field in Eq. (1) is given by hydrostatic, capillary and disjoining contributions:

$$p = \rho\, g\, (h\, \cos\alpha - x\, \sin\alpha) - \sigma\, \kappa - \Pi \tag{2}$$

where x represents the plate downhill direction, κ is the free surface curvature and Π the disjoining pressure.

The small-slope approximation leads to $\kappa = \nabla^2 h$, which is mostly used in literature works involving 2D simulations of thin liquid layers.

The disjoining pressure, related to inter-molecular forces between liquid and solid substrate, was

defined by Schwartz and Eley [10] as:

$$\Pi = B\left[\left(\frac{\delta}{h}\right)^n - \left(\frac{\delta}{h}\right)^m\right] \tag{3}$$

$$B = \frac{(n-1)(m-1)}{n-m}\frac{\sigma}{\delta}(1-\cos\theta_e) \tag{4}$$

where $1 < m < n$, δ is the precursor film thickness and θ_e is the equilibrium contact angle.
Zhao and Marshall, [12], observed that values of δ larger than the physical one lead to inaccurate results. Thus, the following correction factor was introduced in Eq. (4):

$$f = 1 + 6.069\,\delta + 161.7\,\delta^2 - 1547\,\delta^3 + 5890\,\delta^4 \tag{5}$$

Disjoining pressure allows for the modeling of the contact line dynamics, but the allowed contact angle is still limited due to the small-slope approximation.
The proper equation defining the capillary pressure can be obtained writing the membranal equilibrium in the normal direction of the free surface, see Appendix, which gives:

$$\kappa = \frac{1}{r_x}\left[\frac{1+\left(\frac{\partial h}{\partial x}\right)^2}{1+\left(\frac{\partial h}{\partial x}\right)^2+\left(\frac{\partial h}{\partial y}\right)^2}\right]^{1/2} + \frac{1}{r_y}\left[\frac{1+\left(\frac{\partial h}{\partial y}\right)^2}{1+\left(\frac{\partial h}{\partial y}\right)^2+\left(\frac{\partial h}{\partial x}\right)^2}\right]^{1/2} \tag{6}$$

where r_x and r_y can be calculated according to Young-Laplace equation:

$$r_x = \frac{\frac{\partial^2 h}{\partial x^2}}{\left[1+\left(\frac{\partial h}{\partial x}\right)^2\right]^{3/2}}\ ;\ r_y = \frac{\frac{\partial^2 h}{\partial y^2}}{\left[1+\left(\frac{\partial h}{\partial y}\right)^2\right]^{3/2}} \tag{7}$$

The fourth order, non-linear PDEs, Eqs. (1) and (2), are solved numerically on the 2D domain of the inclined plate. The following relation:

$$\kappa = \frac{1}{r_x} + \frac{1}{r_y} \tag{8}$$

is used in current simulations for calculating the capillary pressure instead of Eq. (6). However, two versions of the solver FVM code are available, with both Eqs. (6) and (8) implemented, but the simplified relation, Eq. (8), is chosen since the two versions lead to similar results but the computational cost is lower if Eq. (8) is implemented.
The case of gravity and shear acting in the same direction is considered, allowing to correlate the average velocity u_∞ and the thickness h_∞ of the undisturbed film according to [16]:

$$u_\infty = \frac{\rho\, g\, \sin\alpha}{3\,\mu}{h_\infty}^2 + \frac{\tau}{2\,\mu}h_\infty \tag{9}$$

3. Space and time discretization

The 2D spatial domain $L_x \times L_y$ is discretized using a structured, orthogonal grid composed by $n_x \times n_y$ elements of variable size. The convective term $\nabla \cdot \boldsymbol{Q}$ of Eq. (1) is discretized using Finite Volume Method, via a first order upwind scheme. Hence, the flux $\boldsymbol{Q}$ is decomposed into two contributions: $\boldsymbol{Q}^+ = \boldsymbol{u}^+ h$ refers to the the wave propagation with positive velocity, while $\boldsymbol{Q}^- = \boldsymbol{u}^- h$ refers to the wave propagation with negative velocity. This discretization ensures

that the pressure gradient on each element face is computed with a centered difference. More details can be found in [16]. The capillary pressure field, Eqs. (7) and (8), is discretized using a second order centered scheme.
An implicit Euler time integration is chosen due to the restrictive stability constraint on the explicit time step, $\Delta t \propto \Delta x^4$. On the structured grid used in the present work, the computational time can be greatly reduced following an Alternate Direction Implicit scheme, which allows to solve two pentadiagonal algebraic systems at each time step instead of one sparse system. The ADI factorization proposed by Witelski and Bowen [17] for numerical resolution of high-order non-linear diffusion equations, which allows to treat explicitly the mixed derivatives of h arising from the capillary pressure gradient, is adopted. Further details on the discretization can be found in [16, 17].

4. Problem setup

The dynamics of a gravity driven film flowing down an inclined plate are investigated, being the simplest configuration for better understanding the hydrodynamics through structured packing, [4]. The case of gravity driven film ($\boldsymbol{\tau} = 0$) is presented.
Along the upper boundary of the domain, $x = 0$, an inlet section of length $L_{in} \in [0, L_y]$ is defined, where the entering film flux is settled to the undisturbed one, $\boldsymbol{Q_{in}} \cdot \hat{\boldsymbol{n}} = u_\infty h_\infty$, and the pressure $p_\infty = \rho\, g\, h_\infty \cos\alpha + \Pi_\infty$ is imposed; outside the inlet section, the entering flux is equal to zero as well as the pressure. Zero flux entering the domain and zero pressure gradient, $\boldsymbol{Q_{in}} \cdot \hat{\boldsymbol{n}} = 0$ and $\nabla p \cdot \hat{\boldsymbol{n}} = 0$, are imposed at the outlet boundary, $x = L_x$.
Two different set of boundary condition on the lateral boundaries $y = 0,\, L_y$ can be used: symmetry boundary condition, $\boldsymbol{Q} \cdot \hat{\boldsymbol{n}} = 0$ and $\nabla p \cdot \hat{\boldsymbol{n}} = 0$, for the simulation of a plate of indefinite extension along y direction, or wall boundary condition, $\boldsymbol{Q} \cdot \hat{\boldsymbol{n}} = 0$ and free surface inclination equal to equilibrium contact angle θ_e, for the simulation of a domain bounded by solid end-walls at $y = 0,\, L_y$. The following equation:

$$\left.\frac{\partial h}{\partial y}\right|_0 = -\frac{\sqrt{1+\left(\frac{\partial h}{\partial x}\right)^2}}{\tan\theta_e}\,,\ \left.\frac{\partial h}{\partial y}\right|_{L_y} = +\frac{\sqrt{1+\left(\frac{\partial h}{\partial x}\right)^2}}{\tan\theta_e} \tag{10}$$

is implemented for imposing contact angle at the lateral boundaries, with $\frac{\partial h}{\partial x}$ calculated by means of a second order centered scheme, using the available values of h in the grid elements next to the domain boundary.
The dry initial condition, i.e. film height equal to the precursor film thickness $h = \delta$ over the whole domain, is used for the current simulations, in order to focus on the wetting dynamics.

5. Validation

First of all, the disjoining pressure model, Eqs. (3), (4) and (5), is validated for a 1D film flowing down an inclined plate. Simulations are run imposing: plate inclination equal to $\alpha = 60°$; equilibrium contact angle in the range $\theta_e \in [30°, 60°]$; precursor film thickness $\delta = 0.05\, h_\infty$; spatial discretization step equal to $\Delta x = 0.05\, h_\infty$. The simulated liquid is 1−methylepiperazine $0.31x$ MPZ, which physical properties are listed in table 1.
Figure 1(a) shows the shape of the capillary ridge, which is self-similar in time and typically appears close to the moving contact line: according to literature [12], higher values of the imposed equilibrium contact angle lead to higher ridge dimensions. In figure 1(b) the dynamic contact angle is computed for different film flow rates and fitted using the Tanner-Hoffman-Voinov formula [12, 18]:

$$\theta^3 = {\theta_e}^3 \left(1 + C\,\frac{\mu\, u_\infty}{\sigma}\right) \tag{11}$$

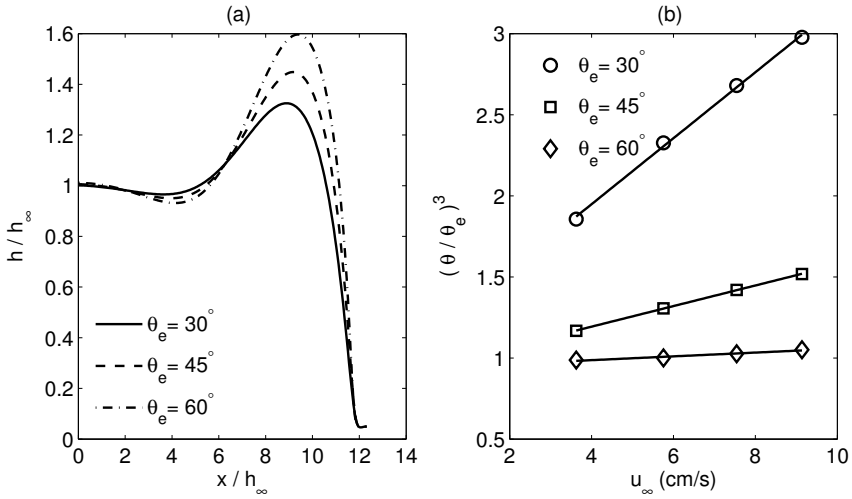

Figure 1. 1D gravity driven film: capillary ridge shape for different equilibrium contact angles θ_e, $Q_{in} = 1\,\mathrm{cm}^2/\mathrm{s}$, $h_\infty = 1.09\,\mathrm{mm}$ (a); dynamic contact angle θ vs undisturbed film velocity u_∞ and imposed equilibrium contact angle θ_e: numerical results (symbols) and Eq.(11) (lines) (b).

where C is the fitting parameter. According to the validation procedure found in [12], it can be stated that surface wettability and contact line dynamics are correctly modeled using disjoining pressure and assuming a thin precursor film, since Eq. (11) well describes the behavior of the dynamic contact angle θ as a function of the undisturbed film velocity u_∞. Moreover, equilibrium contact angle up to $\theta_e = 60°$ had not been investigated (and thus validated) before using disjoining pressure and lubrication theory.

The solver code is then validated with numerical results found in literature, involving rivulets build up. The test case of Singh et al. [4] is chosen for the simulations: $6 \times 5\,\mathrm{cm}^2$ plate, inclined with an angle $\alpha = 60°$ to the horizontal; film flux per unit length $Q_{in} = 1\,\mathrm{cm}^2/\mathrm{s}$ entering through a confined inlet section $L_{in} = 2\,\mathrm{cm}$ at the top of the plate, $\dot{V}_{in} = Q_{in}\,L_{in} = 2\,\mathrm{cm}^3/\mathrm{s}$; 1−methylepiperazine $0.31x$ MPZ liquid simulated (see properties in table 1). It is important to point out that the chosen liquid is used as solvent in packed columns for carbon capture [4].

Thanks to the symmetrical configuration of the problem, only half of the plate is simulated, with symmetry condition imposed at the lateral boundaries $y = 0$, L_y, i.e. an array of parallel rivulets with $2\,L_y$ spacing is simulated. Inlet section is implemented as described in section 4. The precursor film thickness is set to $\delta = 0.025\,h_\infty$. A grid dependence analysis suggested to impose spatial discretization step, which is kept uniform over the computational domain for the rivulet build up simulations, of about $0.075 - 0.1\,h_\infty$, depending on the imposed equilibrium contact angle, which is varied in the range $\theta_e \in [20°, 60°]$.

Figure 2, which shows how the stationary liquid layer distribution changes with the surface wettability, clearly proves that the higher the imposed equilibrium contact angles, the narrower the shape of the rivulet, according to the numerical results of Singh et al. [4].

A proper validation is possible computing the wetted area A_{wet}, which is defined as the portion of plate covered by a layer of liquid with height higher than the precursor film one, and the interface area A_{int}, which is the area of the liquid-gas free surface in the wetted region. In figures 3(a) and 3(b) the resulting trends of A_{wet} and A_{int} as a function of θ_e are compared with the numerical results of Singh et al. [4], obtained by means of a fully 3D model: the correspondence is satisfactory for all the investigated values of θ_e.

According to [19], the liquid pressure of a stable rivulet flowing over an inclined plate is independent of the plate downhill direction x, thus the rivulet profile can be calculated solving

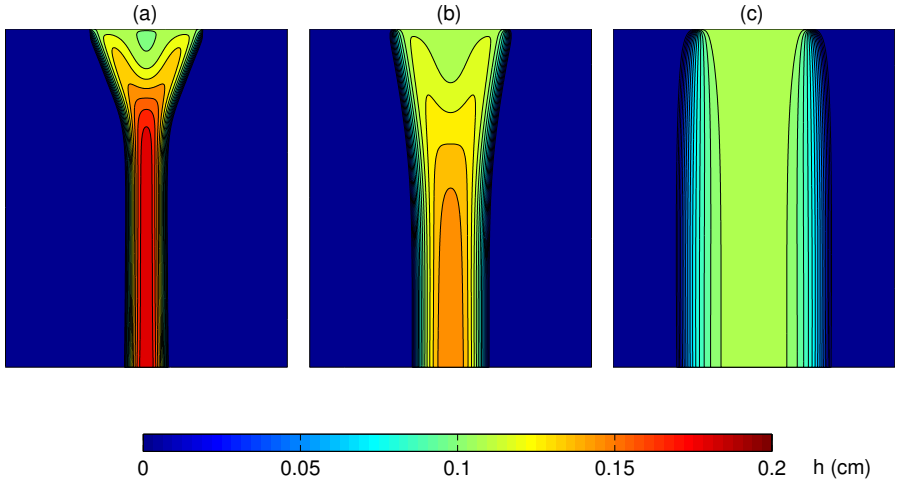

Figure 2. Stationary rivulet distribution over the inclined plate for: $\theta_e = 60°$ (a), $\theta_e = 40°$ (b), $\theta_e = 20°$ (c). $\alpha = 60°$, $\dot{V}_{in} = 2\,\mathrm{cm}^3/\mathrm{s}$.

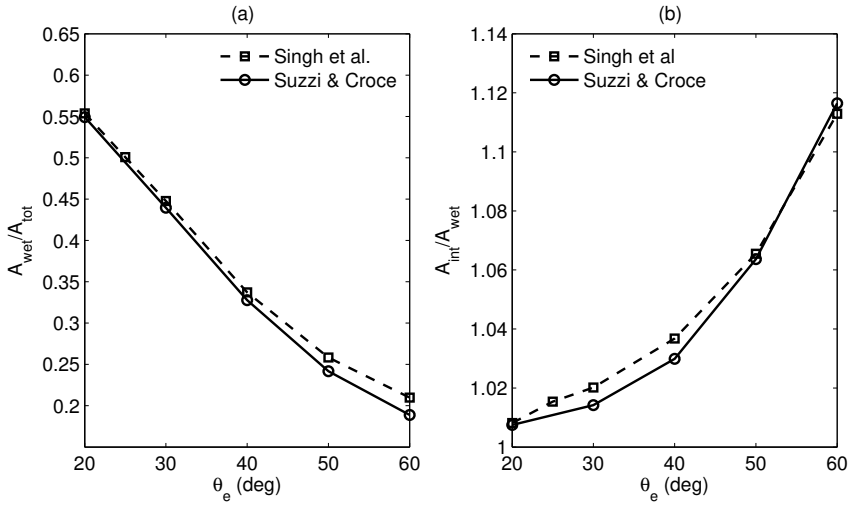

Figure 3. Normalized wetted area of the rivulet as a function of the equilibrium contact angle (a). Normalized interface area of the rivulet as a function of the equilibrium contact angle (b). $\alpha = 60°$, $\dot{V}_{in} = 2\,\mathrm{cm}^3/\mathrm{s}$.

the following initial value problem:

$$p = \rho\, g\, h\, \cos\alpha - \sigma\, \frac{\partial^2 h}{\partial y^2} \left[1 + \left(\frac{\partial h}{\partial y}\right)^2\right]^{-3/2} = \text{const} \tag{12}$$

$$h|_{y_0} = 0,\ \left.\frac{\partial h}{\partial y}\right|_{y_0} = \tan\theta_e \tag{13}$$

The solution of Eq. (12) together with the initial conditions is iterated: the value of the rivulet pressure p is updated at each iteration, until the liquid flow rate, which can be calculated

integrating the film flux per unit length

$$Q = \frac{\rho\, g\, h^3\, \sin\alpha}{3\,\mu} \tag{14}$$

along the rivulet length, equals the imposed one $\dot{V}_{in} = Q_{in}\, L_{in}$. The resulting profile is then compared with the numerical one, obtained cutting the stationary liquid layer distribution at $x = L_x$. The validation for $\theta_e = 60°$ is shown in figure 4, which shows almost a perfect correspondence between numerical results and Eq. (12).

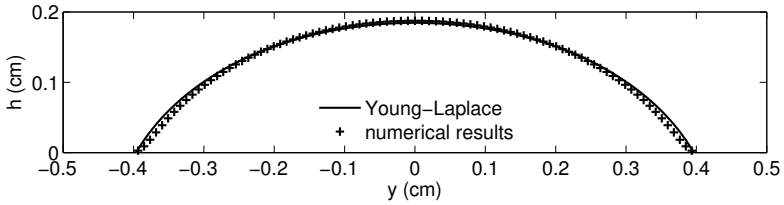

Figure 4. Comparison between rivulet profiles from solution of Eq. (12) and numerical simulation of rivulet build up. $\theta_e = 60°$, $\alpha = 60°$, $\dot{V}_{in} = 2\,\mathrm{cm}^3/\mathrm{s}$.

6. Application to CO_2 absorption

Liquid	$\rho\,(\mathrm{kg\,m^{-3}})$	$\mu\,(\mathrm{Pa\,s})$	$\sigma\,(\mathrm{N\,m^{-1}})$	Ka
$0.31x$ MPZ	981.31	0.03642	0.03480	14.8
$0.41x$ MPZ	962.20	0.02348	0.03589	24.6
$0.51x$ MPZ	946.41	0.01336	0.03437	49.7

Table 1. Physical properties of 1−methylepiperazine (MPZ) at $T = 25°\mathrm{C}$ and $p = 1\,\mathrm{atm}$.

The first step for understanding the hydrodynamics of absorption/distillation processes through structured packing is the analysis of the wetting dynamics of an inclined plate covered by a thin liquid layer. As explained in [4], the wetting phenomenon is dictated by several parameters, making crucial to focus on identifying proper non-dimensional numbers. The effect of solvent properties is analyzed through Kapitza number:

$$\mathrm{Ka} = \sigma \left(\frac{\rho}{\mu^4\, g}\right)^{1/3} \tag{15}$$

The flow characteristics are studied in terms of Weber number:

$$\mathrm{We} = \frac{\rho\, {u_\infty}^2\, h_\infty}{\sigma} \tag{16}$$

which represents the ratio between liquid inertia and surface tension force. The effect of surface wettability is obviously given by the equilibrium contact angle θ_e. The wetted area A_{wet}, which is here normalized to the plate area A_{tot}, is used for describing the wetting process, since it is the parameter to be optimized when designing the corrugated sheets composing the packed column.

Similarly to the approach of Singh et al. [4] and Hoffmann [5], an inclined plate is considered: the lateral boundaries are treated as walls, which implementation is explained in section 4; the whole top boundary of the plate represents the inlet section; the case of gravity driven flow is considered. The effect of θ_e, Ka and We on wetting dynamics are investigated, with equilibrium contact angle and Weber number up to 60° and 0.25 respectively. The Reynolds number is limited to $\mathrm{Re} \leq 5.58$, according to lubrication theory validity. The liquids listed in table 1 are simulated. The choice of these liquids is not casual, since they are used as solvent in CO_2 capture through packed column [4]. A $3 \times 3\,\mathrm{cm}^2$ plate, inclined at an angle $\alpha = 60°$ to the horizontal, is considered, but only half of the plate is simulated, thanks to the symmetry of the problem. The imposed precursor film thickness is equal to $\delta = 0.025\, h_\infty$. The spatial discretization step is not uniform over the computational domain, since a finer grid is required close to the wall for a better description of the liquid behavior, especially when low contact angles are imposed, leading to higher slopes.

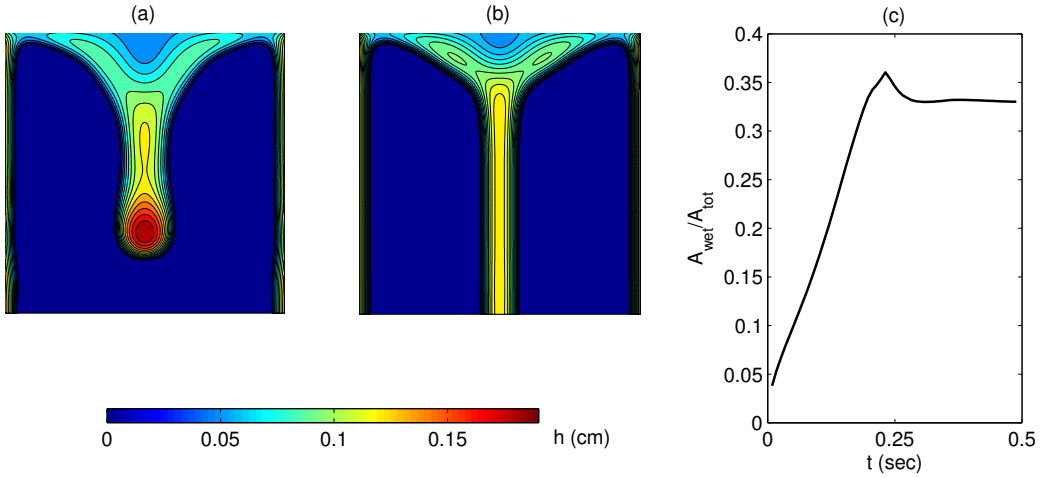

Figure 5. Liquid layer distribution over the inclined plate at $t = 0.19\,\mathrm{s}$ (a) and stationary distribution, $t = 0.49\,\mathrm{s}$ (b). Normalized wetted area as a function of time (c). $\theta = 60°$, $\mathrm{Ka} = 49.7$, $\mathrm{We} = 0.0736$.

Figures 5(a) and 5(b), which refer to the same simulation, show the distribution of liquid $1-$methylepiperazine $0.51x$ MPZ over the plate at two different times. It can be noticed that the lateral walls capture some liquid due to capillary effect, perturbing the undisturbed flow. If the inlet flow rate is too low, this phenomenon leads to the growth of dry-patches on the plate, with the liquid forming two rivulets close to the walls and one rivulet in between. Similar results were obtained experimentally by Hoffman [5] and numerically by Singh et al. [4]. In figure 5(c) the plate wetted area is shown as a function of time. The wetting process can be clearly divided into two regimes: first the liquid bulk, driven by gravity, spreads in downhill direction; after the bulk reaches the outlet section, the contact line dynamics are mainly driven by the capillary force and thus influenced by the surface wettability.
The dependence of the plate wetted area on Weber number, Kapitza number and equilibrium contact angle is shown in figures 6(a) and 6(b). Results refer to the stationary solution of Eqs. (1) and (2). In particular, figure 6(a) suggests that the effect of fluid inertia, i.e. of We, on wetting process grows with the Kapitza number, since the whole coverage of the plate, $A_{wet}/A_{tot} = 1$, is reached for higher values of the Weber number. Thus, liquid spreading over the inclined plate is mainly driven by viscous, surface tension and gravity forces only for low Ka. Figure 6(a) also gives some information about the critical flow rate, defined as the minimum flow rate leading to

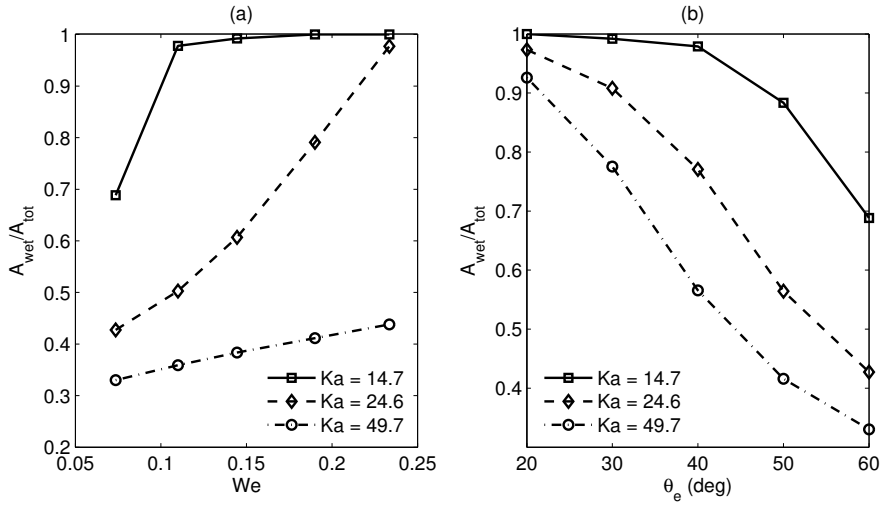

Figure 6. Normalized wetted area at the stationary liquid distribution as a function of Weber number, $\theta_e = 60°$ (a); as a function of equilibrium contact angle, We = 0.0736 (b). Fluids listed in table 1 are simulated, plate inclination is fixed to $\alpha = 60°$.

whole coverage of the plate: the critical value of Weber number (which defines univocally the critical flow rate) can be traced as a function of the Kapitza number of the liquid. The definition of the critical flow rate is crucial, since it defines the most suitable condition (maximum wetted area) for absorption process through structured packing. The surface wettability also has a great impact on wetting process, as shown in figure 6(b): higher values of the equilibrium contact angle lead to lower stationary wetted area, with low changes in contact angle leading to significantly differences in liquid behavior. Similar results were obtained by the rivulet build up simulations, figure 3(a).

Finally, it is important to point out that the computational cost of the presented simulations is limited, thanks to the implemented ADI method, which allows to reach time step Δt up to 10^6 the explicit one. As an example, Singh et al. [4] conducted VOF simulations on a similar setup, running on 128 cores in parallel with 144 h required for a single simulation, while in the present work simulation time is 4 times lower using a single core.

7. Conclusion

An implicit FVM code was implemented in order to solve the 2D lubrication equation describing the evolution of a thin layer of liquid. It was shown that the model is able to compute the film height over the whole domain and capture the contact line dynamics, thanks to the disjoining pressure and the assumption of a thin precursor film. Thus, the 2D approach provides a full analysis of the wetting of a solid substrate, without loss of information comparing to a 3D approach. The fully implementation of capillary pressure allows to investigate values of the equilibrium contact angle up to 60°, which had never been analyzed using lubrication theory before. The code was first successfully validated with literature results for the rivulet build up over an inclined plate. Then, the wetting dynamics of a film flowing down an inclined plate were studied, focusing on the effect of surface wettability, liquid properties (Ka) and flow characteristics (We). The chosen setup and the simulated liquids are directly involved in CO_2 absorption through structured packing. Other numerical works involving distillation/absorption process through packed columns are available in literature, but a fully 3D approach was used by the authors. The advantage of the presented 2D approach is that a whole analysis of the wetting

phenomenon is possible with a gain in terms of computational costs of around two orders of magnitude.
The implemented model also allows to simulate shear driven films, involved in a number of engineering problems. More complex geometries, which are required for fully understanding the liquid behavior over the corrugated sheets involved in structured packing, can also be simulated using the solver code, even in the present structured grid form. It was not possible to simulate high Kapitza number solvents, as done in [4,5], because the low viscosity leads to higher values of the Reynolds number, which are not allowed by the current assumption of neglecting liquid inertia. However, lubrication theory is still valid, keeping liquid inertia terms during the integration of Navier-Stokes equations along plate normal direction.

Appendix

The mathematical procedure for obtaining Eq. (6), which allows to define properly the disjoining pressure term, is derived in this Appendix.

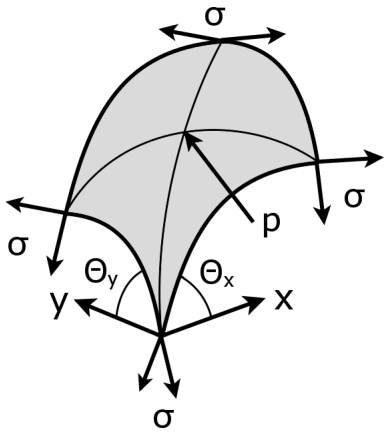

Figure A1. Forces acting on a control volume of free surface.

Consider the portion of free surface shown in figure A1. Assuming low stretching of the control surface (i.e. the corner angles are close to 90°), the membranal equilibrium along the normal direction $\hat{\boldsymbol{n}}$ between the surface tension force and the capillary pressure gives:

$$p\,dA = \sigma\,\sin\left(d\beta_x\right)\,\cos\Theta_y\,r_y\,d\beta_y + \sigma\,\sin\left(d\beta_y\right)\,\cos\Theta_x\,r_x\,d\beta_x \tag{A.1}$$

where $r_{x,y}$, $\Theta_{x,y}$ and $d\beta_{x,y}$ are the radii of curvature, the free surface slopes and the arc angles, calculated along the Cartesian directions.
The free surface area dA, subjected to the capillary pressure p, can be expressed as:

$$dA = \left(r_x\,d\beta_x\right)\,\left(r_y\,d\beta_y\right)\,\sqrt{1-\sin^2\Theta_x\,\sin^2\Theta_y} \tag{A.2}$$

Assuming $\sin d\beta_{x,y} \simeq d\beta_{x,y}$ and dividing both LHS and RHS of Eq. (A.1) for $\sigma\,dA$ lead to:

$$\kappa = \frac{p}{\sigma} = \frac{1}{r_x}\,\frac{\cos\Theta_y}{\sqrt{1-\sin^2\Theta_x\,\sin^2\Theta_y}} + \frac{1}{r_y}\,\frac{\cos\Theta_y}{\sqrt{1-\sin^2\Theta_x\,\sin^2\Theta_y}} \tag{A.3}$$

Using the definitions of the free surface slopes $\Theta_{x,y}$:

$$\tan\Theta_x = \frac{\partial h}{\partial x},\ \tan\Theta_y = \frac{\partial h}{\partial y} \tag{A.4}$$

the terms $\cos\Theta_{x,y}$, $\sin\Theta_{x,y}$ can be expressed as a function of $\frac{\partial h}{\partial x}$, $\frac{\partial h}{\partial y}$ and Eq. (A.3) recast, giving Eq. (6).

References

[1] De Candido E, Croce G and D'Agaro P 2012 *Heat Transfer Eng.* **33** 1130
[2] Croce G, Candido E D, Habashi W G, Munzar J, Aube M, Baruzzi G S and Aliaga C 2010 *J. Aircraft* **47** 1283
[3] Bourgault Y, Habashi W G, Dompierre J and Baruzzi G S 1999 *Int. J. Numer. Methods Fluids* **29** 429
[4] Singh R K, Galvin J E and Sun X 2016 *Chem. Eng. Sci.* **142** 244
[5] Hoffmann A, Ausner I, Repke J U and GWozny 2005 *Comput. Chem. Eng.* **29** 1433
[6] Subramanian K and Wozny G 2012 *Int. J. Chem. Eng.* **2012** 13
[7] Repke J U, Ausner I, Paschke S, Hoffmann A and Wozny G 2007 *Chem. Eng. Res. Des.* **85** 50
[8] Xu Y Y, Zhao M, Paschke S and Wozny G 2014 *Ind. Eng. Chem. Res.* **53** 7797
[9] Sellier M 2015 *Int. J. Multiphase Flow* **71** 66
[10] Schwartz L W and Eley R R 1998 *J. Colloid Interface Sci.* **202** 173
[11] Weidner D E, Schwartz L W and Eres M H 1997 *J. Colloid Interface Sci.* **187** 243
[12] Zhao Y and Marshall J S 2006 *J. Fluid Mech.* **559** 355
[13] Lemaitre C, Hemon P and de Langre E 2007 *J. Wind Eng. Ind. Aerodyn.* **95** 1259
[14] Diez J A and Kondic L 2002 *J. Comput. Phys.* **183** 274
[15] Mata M R and Barozzi A L 2011 *J. Comput. Phys.* **230** 6334
[16] Suzzi N and Croce G 2017 *J. Phys. Conf. Ser.* **796** 012038
[17] Witelski T P and Bowen M 2003 *Appl. Numer. Math.* **45** 331
[18] Blake T D 2006 *J. Colloid Interface Sci.* **299** 1
[19] El-Genk M S and Saber H H 2001 *Int. J. Heat Mass Transfer* **44** 2809